

The role of stepped surfaces on the magnetotransport in strained thin films of $\text{La}_{0.67}\text{Ca}_{0.33}\text{MnO}_3$

C. Beekman and J. Aarts.

Kamerlingh Onnes Laboratory, Leiden University, P.O. Box 9504, 2300 RA Leiden, the Netherlands

Abstract. We report a comparative study of the properties of very thin films of $\text{La}_{0.67}\text{Ca}_{0.33}\text{MnO}_3$ grown epitaxially under strain on flat SrTiO_3 (STO) and on 1° -miscut STO. For the films on flat STO the transport properties show well-known behavior, namely values of the metal-insulator transition temperature which are strongly reduced with respect to the bulk value. The reduction in films on miscut STO is significantly less strong than in films on flat STO, even though they appear similar as to strain state. Moreover, the residual resistance at low temperatures is lower than for the case of flat films. Magnetically, we find reduced values of the saturation magnetization with respect to the bulk value, indicating the presence of a dead layer in both cases. We argue that the higher density of the step edges on the miscut substrates lead to strain relaxation in the form of point defects and an increased electronic bandwidth, which actually make the electronic properties more robust.

PACS numbers:

1. Introduction

Transition metal oxides with the perovskite structure are strongly correlated electron systems which show diversity in physical properties caused by the competition between charge, spin and orbital degrees of freedom. Much work has been done in the last decade to understand the underlying physics of the correlated and semi-localized 3d electrons and their interaction with the lattice. In particular for the manganites, showing the colossal magnetoresistance effect (CMR) connected to the combined metal-insulator (MI) and paramagnetic-to-ferromagnetic transition, much progress has been made, as can be found in a number of reviews [1, 2, 3]. Still, even in bulk materials the picture is still being refined, as was for instance shown recently in the discovery of the existence of glassy correlated phases in single crystals[4] and thin films[5] of optimally doped $\text{La}_{0.7}\text{Ca}_{0.3}\text{MnO}_3$. For thin films, a large amount of work has gone into basic questions on their physical properties, with the possibility of strain and interface engineering as issues of special interest. In bulk manganites of the type $(\text{RE}_{1-x})\text{A}_x\text{MnO}_3$ (RE is a 3+ Rare Earth ion, A is a 2+ alkaline ion) and at fixed RE to A ratio and therefore the Mn^{3+} to Mn^{4+} ratio, the properties can be changed by varying the radius of the 2+ ion[6, 7]. This is basically because the ion radius influences the structure of the coupled network of MnO_6 octahedra, which changes the balance between the itinerancy of the Mn 3d electrons, and the strength of the Jahn-Teller distortions which tend to trap electrons on the Mn sites. In films this effect can be amplified by growing on a substrate with a different lattice parameter, thereby putting the film under tensile or compressive strain. For instance in films of $\text{La}_{0.7}\text{Ca}_{0.3}\text{MnO}_3$ (LCMO; pseudocubic lattice parameter $a_c = 0.386$ nm) on SrTiO_3 (STO; $a_c = 0.391$ nm) the temperature of the metal-insulator transition T_{MI} goes down to 110 K for films with a thickness of around 10 nm, compared to a bulk value of 260 K [8, 9, 10, 11]. Below about 5 nm the MI transition rather abruptly disappears, mainly because the large strain leads to different crystal structures in the film [11]. At the same time, magnetic measurements indicate the presence of a dead layer in the LCMO/STO system[12, 13] of a few nm and nanoscale phase separation [10], and also in general a lowered value of the saturation magnetization for larger thicknesses [8].

Gaining more understanding about these ultrathin films in the regime around 10 nm is of interest, in particular since the highly polarizable STO allows gating of the devices. In this regard, the role of defects on the substrate surface, such as atomic steps, on the electronic properties, have yet received very little attention. Here we present a comparative study of LCMO films grown on flat SrTiO_3 (STO; tensile strain) and on miscut STO substrates, which shows that such steps can have a significant influence, and are beneficial to several useful electronic properties. The miscut substrates have an intentional misorientation of the surface normal of 1° towards the [010] direction, which leads to terraces of about 25 nm. We use the miscut to investigate the sensitivity of film properties to local variations of substrate surface and thus probing the effect of local strain relaxation and disorder. From high resolution transmission microscopy

(HR-TEM) we find that basically all films show the bulk $Pnma$ structure, with no clear differences between the microstructures of films grown on flat and miscut STO. From transport data we find that these film show the same trends in T_{MI} as found before, with a strong drop for films on flat STO, and reaching a value of 110 K around a thickness of 10 nm. For films on miscut STO, T_{MI} stays significantly higher, not coming below 140 K, but the low temperature resistivity in the metallic state is found to be lower than for the films on flat surfaces. We also discuss the issue of magnetization and show that the saturation values for films in this thickness regime are often lower than can be expected on the basis of a simple dead layer picture. We distill the following physical picture. The high density of the step edges leads to strain relaxation in the form of point defects, and thereby to an increased electronic bandwidth, with a higher T_{MI} and lower resistivity. The presence of steps therefore, somewhat counter intuitively, has a stabilizing effect on the electronic properties, and leads to more effective charge transport.

2. Experimental

Epitaxial films of LCMO with thicknesses between 47 nm and 6 nm were grown on (001) STO substrates, by DC sputtering in oxygen pressure of 300 Pa at a growth temperature of 840 °C. The substrates have a misorientation of either $<0.2^\circ$ in random direction, which we denote as flat STO, or 1° towards [010] direction. Here we define the nomenclature which we will use throughout this paper to refer to our films. Films grown on flat STO are indicated by $L(d)$, with d the film thickness (rounded to the nearest integer value), and films grown on misoriented STO by $L(d)_{mis}$. Before and after film growth we used Atomic Force Microscopy (AFM) to asses the quality of the STO substrate and the LCMO film (see Fig.1). All films show clear unit-cell high step edges. The films grown on flat STO show an average terrace length of 75 nm and the films grown on misoriented STO show an average terrace length of 20 nm, identical to the terrace length of the substrate (see Fig.1). The thickness, growth rate and lattice parameters of the LCMO films were determined by x-ray reflectivity (XRR) and reciprocal space mapping (RSM) measurements, respectively[14]. The average growth rate of our LCMO thin films is 0.8 nm/min, which results in films with roughness of the order of the dimensions of the unit cell.

We have characterized the microstructure using HR-TEM. The specimens were prepared according to a standard cross-section preparation method. Before insertion into the microscope, the specimens were plasma-cleaned for 1 minute to prevent carbon contamination during the experiments. The analysis was performed with a FEI TITAN equipped with a spherical aberration (Cs) corrector and a High Resolution Gatan Image Filter (HR-GIF) operated at 300kV. HR-TEM investigations on several specimens for each film confirm that our films are epitaxial. The perovskite crystal structure of the films is close to cubic with lattice parameter $a_c = 0.39$ nm, but due to small rotations of the oxygen octahedra it becomes orthorhombic (space group: $Pnma$). Using electron diffraction we observed that throughout the films the bulk $Pnma$ structure is present

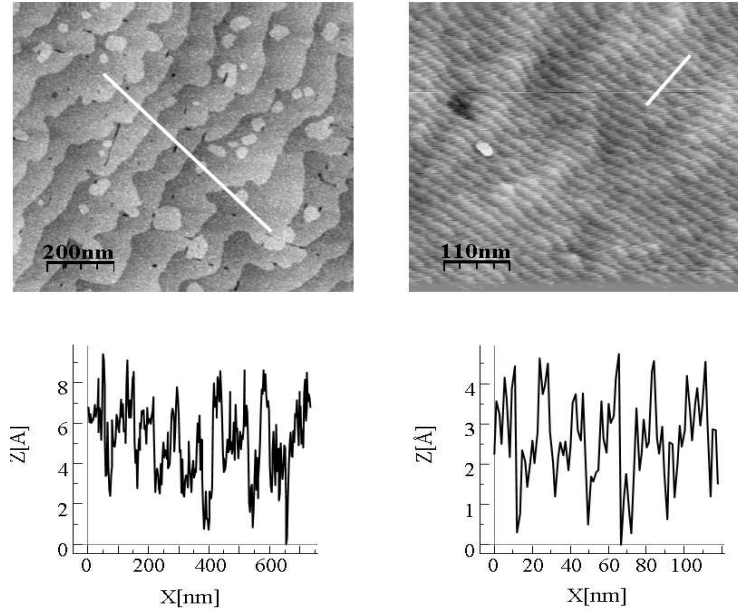


Figure 1. AFM images of LCMO films and corresponding profiles of (left) 15 nm LCMO on flat STO, L(15) (scale bar: 200 nm), and (right) 7 nm LCMO on STO with a misorientation of 1° towards the $[010]$ direction, L(7)_{mis} (scale bar: 100 nm).

with lattice parameters of $\sqrt{2}a_c$, $2a_c$ and $\sqrt{2}a_c$. For most films, the b axis was found to be parallel to the interface normal (with length $2a_c$ in pseudocubic notation [14]). In HR-TEM mode (see Fig.2), and scanning along the interface, we did not observe any antiphase boundaries or any domain type disorder, which is in line with previous reports [15]. The amorphous layer visible at the top surface of the thin film in Fig.2 (top image) is glue used during preparation of the sample. The HR-TEM images shown in Fig.2 (samples L(6), L(10) and L(7)) all show a fully epitaxial thin film. There is a special reason to show a micrograph for sample L(10), since this film has deviating properties compared to the typical film on flat STO, as will be shown later. HR-TEM on this film showed no differences compared to the other films. We also find that films grown on 1° misoriented STO (Fig.2c) are epitaxial with no clear influence of the step edges on the microstructure of the LCMO film. We also do not observe any misfit dislocation at the film-substrate interface in any of the films, which were investigated with HR-TEM.

The magnetotransport properties were studied by measuring the current (I) - voltage (V) characteristics as function of temperature and in high magnetic fields. We used a PPMS (Physical Properties Measurement System, Quantum Design) for temperature control ($T = 20 - 300$ K) and for magnetic field control ($H_a = 0 - 9$ T), in combination with an external current source and nanovoltmeter. The films were patterned into microbridges[16] to determine the low temperature resistivity. For the magnetization measurements we used an MPMS (Magnetic Properties Measurement System, Quantum Design) with $T = 10 - 300$ K and $H_a = 0 - 5$ T.

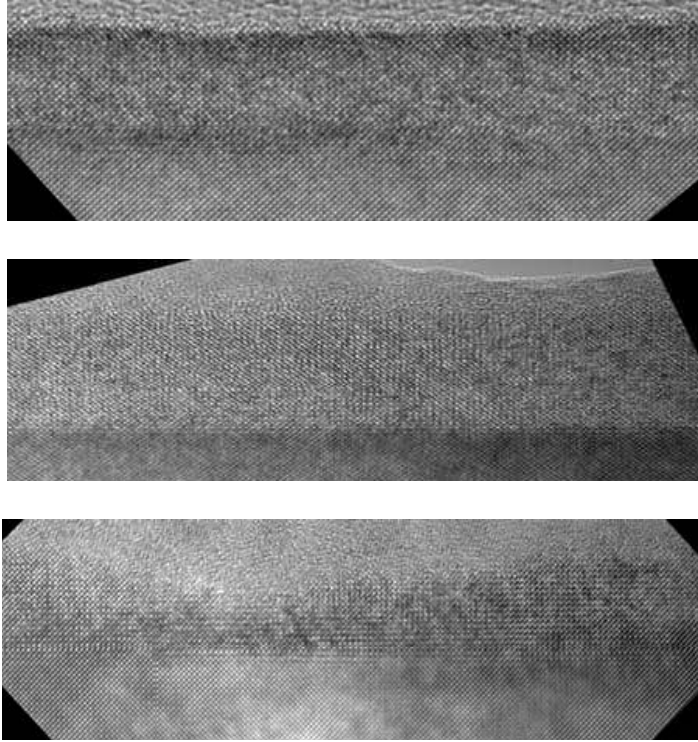


Figure 2. HR-TEM micrographs of LCMO films on STO, from top to bottom L(6), L(10), L(7)_{mis}. The atom columns which are clearly visible in all cases set the scale.

3. Transport properties

We measured the I - V characteristics in a temperature range of 20 - 300 K for films with varying thicknesses between 6 - 20 nm. For films on both flat and miscut substrates the I - V curves were mostly linear, except in a small range around the transition, where weak non-linearities were found. In Fig.3 we show the temperature dependent resistance $R(T)$ for three LCMO films grown on flat STO, as determined at an applied current I of 0.1 μA . The films show a clear metal-insulator transition accompanied by a resistance drop of three orders of magnitude. All films show typical CMR effect, a reduction in resistance of a few orders of magnitude upon application of a 5 T magnetic field. For L(20) the transition temperature T_{MI} , which corresponds to the maximum resistance

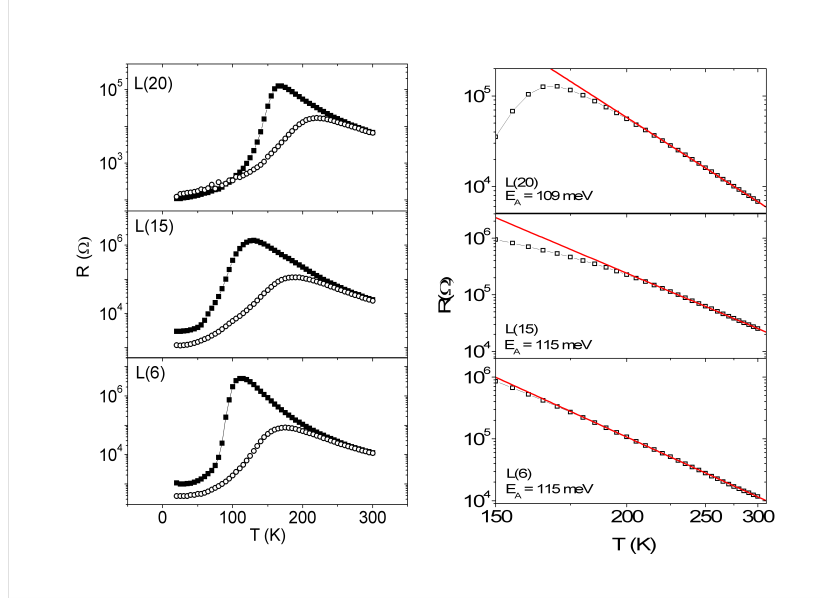


Figure 3. (Left) resistance R vs. temperature T for samples L(20) (top panel), L(15) (center panel) and L(6) (bottom panel) as determined from the I-V curves at an applied current of $0.1 \mu\text{A}$. Squares: zero field; circles: $H_a = 5$ T. (Right) $\log R$ vs. T in the temperature range 150 - 300 K for the same samples. Note: the scale on the T-axis is reciprocal in order to show the $1/T$ -behavior. The fit to extract the activation energy (E_A) of the polaron hopping process is also shown (solid lines).

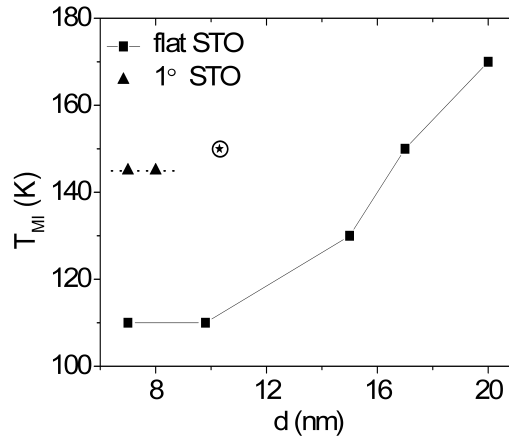


Figure 4. The dependence of T_{MI} on film thickness for LCMO films grown on flat (squares + star) STO and 1° misoriented STO (triangles). The star designates sample L(10). Drawn and dashed lines are guides to the eye.

value, is 170 K, which occurs approximately 100 K below T_{MI} for bulk LCMO. T_{MI} is further reduced when the film becomes very thin, L(6) shows the transition at $T_{MI} = 110$ K, which is 60 K below T_{MI} for L(20). The dependence on film thickness of

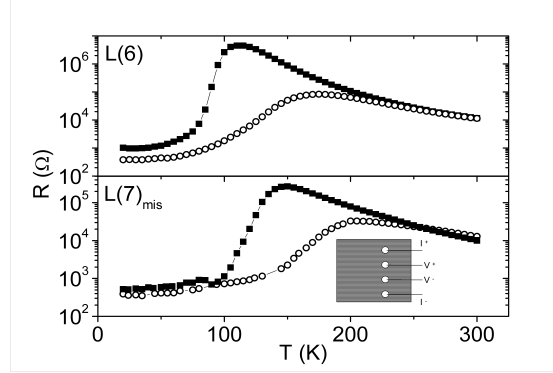


Figure 5. Resistance vs. temperature behavior of sample L(6) (also shown in Fig. 3) and of $L(7)_{mis}$. For the films on misoriented STO the transport properties were measured with the current directed perpendicular to the step edges (see inset for measurement geometry). The resistance values were determined from the I-V curves at an applied current of $0.1 \mu\text{A}$. The squares denote zero field; circles: $H_a = 5 \text{ T}$.

T_{MI} is shown in Fig.4. For films grown on flat STO the metal-insulator transition is steadily shifted to lower temperature as the film thickness is reduced. However, the film L(10) (indicated by \star in Fig.4) grown on flat STO deviated from this trend. There is a connected observation in the magnetization measurements, which we will discuss below.

In the paramagnetic state, $R(T)$ is expected to show activated behavior. In Fig.3 (right panel), we plot $\log R$ vs. T (with the T -axis reciprocal to show the $1/T$ -behavior). A linear fit to the data provides the activation energy (E_A) for the polaron hopping process. For most films the high temperature data show activated behavior with $E_A = 110 - 120 \text{ meV}$ (see Table 1), independent of the film thickness, which is in the accepted range of values for this temperature regime[17]. Deviations typically set in around $1.3 \times T_{MI}$ (for example see sample L(15) center panel Fig.3). In this respect at least, the thin films do not behave different from bulk material. However, what happens in the transition of such strained ultrathin films does not coincide with the simple picture of variable range polaron hopping[19, 20]. Indeed, several studies have shown the formation of an intervening phase consisting of glassy polaron regions[4, 5] as the system is warmed through the MI-transition. Moreover, we found earlier that the dimensions of these correlated (static) polaron regions are sensitive to the strain state of the films[5].

A novel feature of our studies is the investigation of the effect of unit-cell high step edges on the STO substrate surface on the thin film properties. For these films the transport properties were measured in a four-point geometry with the current directed perpendicular to the step edges (see inset Fig.5). Their thickness was determined from HR-TEM micrographs and is 7 and 8 nm ($L(7)_{mis}$ and $L(8)_{mis}$). $R(T)$ for $L(7)_{mis}$ was measured at $I = 0.1 \mu\text{A}$ and is shown in Fig. 5, with $R(T)$ of L(6) shown for comparison. The observed T_{MI} for both films on 1° STO is 145 K, so T_{MI} is much less reduced than

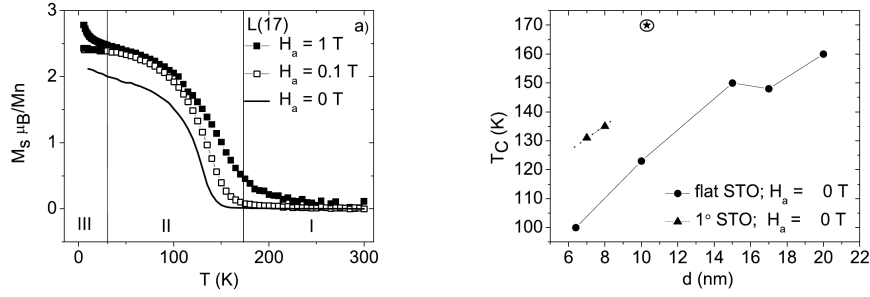


Figure 6. a) M vs. T behavior for L(17). The magnetization was measured in $H_a = 1$ T (closed squares), $H_a = 0.1$ T (open squares) and $H_a = 0$ T (line). b) The Curie temperature as function of film thickness, determined from M vs T at $H_a = 0$ T (circles) and $H_a = 0.1$ T (squares). The triangles show T_C for two films grown on 1° STO and the star shows T_C for sample L(10). The drawn and dashed lines are guides to the eye.

for films on flat STO (see Fig.4, triangles). However, from the HR-TEM and RSM characterization it is clear that the films on misoriented STO are fully epitaxial across the entire film thickness. The lack of reduction in T_{MI} for films on misoriented STO is step-induced but not due to the loss of epitaxial relation with the substrate. It has been shown before that strain relaxation in these materials may occur in the form of dislocations in the film [18]. From HR-TEM we did not observe any dislocations in our thin films, however, point defects should still be present and the amount is possibly enhanced by the presence of the steps. Finally, we mention the values of the residual resistivity (see Table 1), as determined from structured samples. Resistivity values for films on miscut substrates are clearly lower even compared to the thickest films grown on flat substrates.

4. Magnetic properties

Here we present the magnetization behavior of the as-grown films on flat and misoriented STO substrates. Typical behavior of the magnetization M vs. T measured in magnetic fields of $H_a = 0, 0.1$ T, 1 T is shown in Fig.6a for L(17). The Curie temperature was determined from M vs. T , measured in zero magnetic field, by taking the intercept of the constant high temperature magnetization with the linearly increasing $M(T)$. When the film thickness is reduced, we observe that T_C is also shifted to lower temperature as shown in Fig. 6b, and continues to coincide with the temperature of the metal-insulator transition. For the measurement in $H_a = 1$ T we assume that the magnetization is saturated. In the $M(T)$ behavior at 1 T (see Fig. 6a) the magnetization shows a sudden increase below $T = 30$ K. The relative strength of this upturn increases as the film thickness is reduced but the temperature at which the upturn starts is constant. This feature is not an intrinsic feature of the LCMO thin films. From Fig.7 it becomes clear that the M vs. T of a bare STO substrate also shows an upturn below $T = 30$ K.

Apparently, at low T a paramagnetic contribution ($\chi = C/T$, with C the Curie constant) dominates but disappears into the diamagnetic background above $T = 30$ K. We surmise that the emergent paramagnetism is due to the presence of impurities and/or defects in the bulk of the substrate. We have also investigated the field dependent magnetization at $T = 10$ K, shown for L(20) in Fig.7b. From these results we can extract the coercive field and the value for the saturation magnetization (M_s) as function of film thickness. The coercive field varies between ± 6 and ± 15 mT for the different samples. The magnetization is given in units of μ_B per Mn-ion and can be described, at high fields, as $M = M_s + \chi H$ (see inset Fig.7b). The plotted data in the main graph is corrected

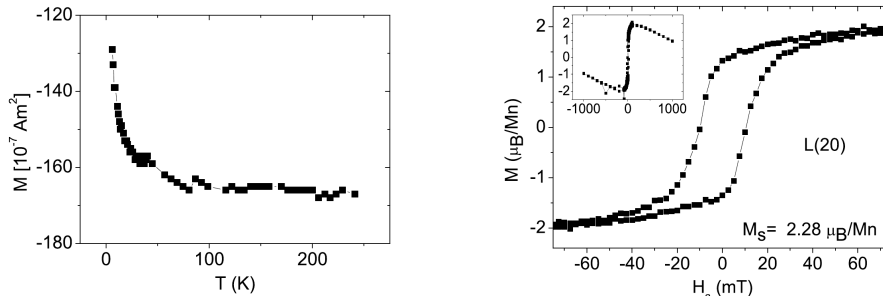


Figure 7. Left: Magnetization as function of temperature for a bare STO substrate measured in $H_a = 1$ T. Right: Magnetization as function of applied magnetic field H_a for the 20 nm thick LCMO film on flat STO. The saturation magnetization M_s at 1 T is $2.28 \mu_B$ per Mn-ion. The inset shows $M(H_a)$ measured up to 1 T.

for the diamagnetic and paramagnetic contribution of the STO substrate by subtracting $\chi \times H_a$ determined at high fields. The values for M_s are determined after correction by taking the value for M at $H_a = 1$ T. The theoretical saturation magnetization for bulk LCMO would be $3.7 \mu_B$ per Mn-ion. For our films we observe slightly fluctuating values for M_s but always low compared to the expected bulk value. For L(20) in Fig.7 the value is $2.28 \mu_B/\text{Mn-ion}$. The lower values indicate that a magnetically dead or weak layer is generally present in our LCMO thin films. The only film showing almost bulk-like saturation magnetization (i.e. no dead layer) is L(10). This coincides with the enhanced value for T_{MI} in this film. Formation of the dead layer is probably sensitive to the initial growth conditions, in particular to the oxygen stoichiometry of the first layers. However, L(10) is the only film that deviates in this respect, since films typically have the dead layer, this makes it hard to investigate this effect further.

5. Discussion

The main observations presented here are that for films on flat STO T_{MI} (T_C) are reduced from the bulk value to a final value of 110 K for film thicknesses below 10 nm. This agrees nicely with the data presented by Bibes et al. [10] on similar strained films and confirms once more the effect of strain on T_{MI} . The novelty here is that fully strained films grown on miscut STO substrates exhibit significantly higher values for

Sample	d nm	a_{in} (Å)	a_{out} (Å)	T_{MI} (K)	T_C (K)	E_A (meV)	M_s (μ_B/Mn)	d_{dead} nm	$\rho(T = 20 \text{ K})$ [$10^3 \mu\Omega\text{cm}$]
L(20)	20	3.90	3.8113	170	160	109	2.28	7.6	1.76
L(17)	17	3.91	3.8135	150	148	114	2.89	3.7	1.53
L(15)	15	3.90	3.8097	130	150	115	1.96	7.0	22.6
L(10)	10.3	3.90	3.796	150	170	114	3.50	0.5	2.44
L(6)	6.4	3.91	3.7979	110	100	115	3.30	0.7	4.46
$\text{L}(8)_{mis}$	8	-	-	145	135	119	2.41	2.8	0.80
$\text{L}(7)_{mis}$	7	3.90	3.7911	145	131	116	2.22	2.8	1.23

Table 1. Summary of the measured values for the thin films presented in this paper. Samples L(20)-L(6): on flat STO; $\text{L}(8)_{mis}$, $\text{L}(7)_{mis}$: on 1° miscut STO. The measured variables are, d : film thickness, $a_{in,out}$: in-plane, out-of-plane lattice parameters, T_{MI} : MI transition temperature, T_C : Curie temperature, E_A : polaron hopping activation energy, M_s : saturation magnetization at $T = 10 \text{ K}$ at 1 T (μ_B/Mn), the corresponding dead layer thickness d_{dead} and the resistivity as determined from transport on microbridges patterned into the thin films[5].

T_{MI} compared to their flat STO counterparts. Transport properties of microbridges patterned into these films (reported elsewhere[5]) show that films grown on miscut substrates also have significantly reduced resistivity values (see table 1). Still, the previously reported strongly nonlinear behavior associated with the correlated polaron formation, as the device is warmed through the MI-transition, is present for all the films in this work. As the film thickness is reduced, the nonlinear behavior becomes more pronounced. Films on miscut STO show the nonlinear behavior in the onset of the transition, with a somewhat reduced intensity compared to film on flat STO with similar thickness.

All the above-mentioned observations in transport lead to the following general picture. We believe that the presence of the step edges lead to disorder (in the form of local defects[18]). Perhaps counterintuitive, since Kumar et al. [21] use the Holstein-Double Exchange model to show that disorder enhancement of the polaron tendency in manganites leads to increased resistivity and *reduction* of T_{MI} . Even more so since from the HR-TEM presented here there is no visible evidence that the miscut alters the epitaxy in any way; nor do we find any defects or dislocations. However, point defects should still be present and could explain the enhanced itinerancy of the miscut samples. Possibly, when the film tends to become insulating the introduction of density of states inhomogeneities, through defects and impurities, results in the formation of additional conduction channels. This is in line with previous reports [22] which show that metallization of an insulating phase of $(\text{La,Ca})\text{MnO}_3$ is possible by introducing valence variation on the Mn-site or by introducing defects in the parent magnetic state. It seems probable that the introduction of disorder also leads to disruption of the formation of the correlated polaron regions, making it harder to form a homogeneous glassy polaron phase.

Next we couple this to the magnetic properties of the films. For all films the MI-transition coincides with T_C , which decreases to a value around 100 K for thicknesses below 10 nm. The films also show reduced values for the saturation magnetization, indicating the presence of a dead layer. It is tempting to connect the dead layer to reported NMR data[10], which showed that a non-ferromagnetic insulating (NFI) phase exists, at least partly, in a region up to 5 nm from the interface. On the other hand, our thinnest films show an almost full saturation magnetization in 1 T. The films with thicknesses of 15 nm and 20 nm show a much lower saturation magnetization (even in 1 T) than might be expected, leading to estimates of a dead layer thickness which are not realistic. The reduction in magnetic moment seems rather due to growth-induced defects, which are antiferromagnetic in nature, but now not easily saturated. This is a similar conclusion as was reached by us before [8], but in contrast to e.g. Ref.[10], and appears to depend on the exact growth conditions of the films. Interestingly, the films on miscut substrates, where relaxation has set in more strongly, also show low values for M_s . More precisely, they show the lower values found in thicker films grown on flat substrates instead of the high values of the thinnest films. This reinforces the argument that the step edges lead to disorder in the form of local defects [18], which then also enhances T_{MI} .

6. Conclusion

In this paper we have presented a comparative study of the magnetotransport properties of ultrathin LCMO films grown on flat and on 1° miscut STO substrates. For flat films, we find the usual strain-induced reduction in T_{MI} (T_C) as the film thickness is reduced. However, for films grown on the miscut substrates we find enhanced values for T_{MI} (and T_C), indicating that strain relaxation has set in more strongly due to the presence of the step-edges. Together with a magnetically dead layer, which is typically present for films on flat and miscut STO alike, we deduce the following physical picture. The presence of the step edges leads to strain relaxation in the form of point defects, leading to an enhanced electronic band width due to induced density of states inhomogeneities. The effect of step edges is therefore somewhat different than might be expected. Instead of adding to the disorder in such a way that the LCMO films are driven towards an insulating state, they actually lead to an electronically more stable situation.

7. Acknowledgements

We thank I. Komissarov for discussions, H. Zandbergen and M. Porcu (National Centre for High Resolution Microscopy, Kavli Institute for Nanoscience, Delft Technical University) for performing the HR-TEM measurements and J.A. Boschker (University of Twente) for performing the RSM measurements. This work was part of the research program of the Stichting voor Fundamenteel Onderzoek der Materie (FOM), which is financially supported by NWO.

- [1] Y. Tokura, Rep. Prog. Phys. **69** 797 (2006); see also Y. Tokura, 'Colossal Magnetoresistive Oxides', Gordon and Breach Science Publishers (2000).
- [2] E. Dagotto, S. Yunoki, C. Sen, G. Alvarez and A. Moreo, J. Phys.: Condens. Matter **20** 434224 (2008); see also E. Dagotto, 'Nanoscale phase separation and Colossal Magnetoresistance', Springer Series in Solid-State Sciences **136** (2003).
- [3] M. B. Salamon, Rev. Mod. Phys. **73**, 583 (2001).
- [4] J.W. Lynn, D. N. Argyriou, Y. Ren, Y. Chen, Y. M. Mukovskii, and D. A. Shulyatev, Phys. Rev. B **76**, 014437 (2007).
- [5] C. Beekman, J. Zaanen and J. Aarts Phys. Rev. B **83**, 235128 (2011)
- [6] A. Machida, M. Itoh, Y. Moritomo, S. Mori, N. Yamamoto, K. Ohoyama, and A. Nakamura, Physica B **281** & **282**, 524 (2000)
- [7] Y. Tokura and Y. Tomioka, C, J Mag. Mag. Mat. **200**, 1 (1999)
- [8] J. Aarts, S. Freisem, and R. Hendrikx, and H.W. Zandbergen, Appl. Phys. Lett. **72**, 2975 (1998).
- [9] K. Dörr, J. Phys. D: Appl. Phys. **39**, R125R150 (2006).
- [10] M. Bibes, Ll. Balcells, S. Valencia, J. Fontcuberta, M. Wojcik, E. Jedryka, and S. Nadolski, Phys. Rev. Lett. **87**, 067210 (2001).
- [11] Z. Q. Yang, R. Hendrikx, J. Aarts, Y. L. Qin and H. W. Zandbergen, Phys. Rev. B **70**, 174111 (2004).
- [12] M. J. Calderón, L. Brey, and F. Guinea, Phys. Rev. B **60**, 6698 (1999)
- [13] S. Valencia, A. Gaupp, and W. Gudat Ll. Abad, Ll. Balcells, and B. Martínez, Appl. Phys. Lett. **90**, 252509 (2007)
- [14] The pseudocubic lattice parameters a (in-plane) and b (out-of-plane) as determined from Reciprocal Space Mapping are shown in Table 1.
- [15] Z.Q. Yang, R. Hendrikx, J. Aarts, Y.L. Qin and H.W. Zandbergen, Phys. Rev. B, **70**, 174111 (2004)
- [16] C. Beekman, I. Komissarov, M. Hesselberth and J. Aarts, Appl. Phys. Lett. **91**, 062101 (2007)
- [17] T.T.M. Palstra, A. P. Ramirez, S-W Cheong, B. R. Zegarski, P. Schiffer J. Zaanen, Phys. Rev. B, **56**, 5104 (1997)
- [18] K. Terai, M. Lippmaa, P. Ahmet and T. Chikyow, T. Fujii, H. Koinuma, and M. Kawasaki, Appl. Phys. Lett. **80**, 4437 (2002)
- [19] G. N. Greaves, J. Non-Crys. Solids, **51**, 87 (1982)
- [20] Y. Sun, X. Xu and Y. Zhang J. Phys. Condens. Matter, **12**, 10475 (2000)
- [21] S. Kumar and P. Majumdar, Phys. Rev. Lett. **96**, 016602 (2006)
- [22] K. Pradhan, A. Mukherjee, and P. Majumdar, Eur. Phys. Lett. **84**, 37007 (2008)